

# A pH-differential Dual-Electrolyte Microfluidic Reactor for Electrochemical Reduction of CO<sub>2</sub>

Xu Lu <sup>1</sup>, Dennis Y.C. Leung <sup>1,\*</sup>, Huizhi Wang <sup>2</sup>, M. Mercedes Maroto-Valer <sup>2</sup>, Jin Xuan <sup>2,\*</sup>

<sup>1</sup> Department of Mechanical Engineering, The University of Hong Kong, Pokfulam, Hong Kong

<sup>2</sup> Centre for Innovation in Carbon Capture and Storage (CICCS), School of Engineering and  
Physical Sciences, Heriot-Watt University, Edinburgh, U.K.

\* Corresponding authors, Tel.: +852 2859 7911, fax: +852 2858 5415, email:

[ycleng@hku.hk](mailto:ycleng@hku.hk) (D.Y.C. Leung); Tel: +44 (0) 131 451 3293; Fax: +44 (0)131 451 3129,

email: [j.xuan@hw.ac.uk](mailto:j.xuan@hw.ac.uk) (J. Xuan)

## Abstract

CO<sub>2</sub> can be converted to useful fuels by electrochemical processes. As an effective strategy to address greenhouse effect and energy storage shortage, electrochemical reduction of CO<sub>2</sub> still needs major improvements on its efficiency and reactivity. Microfluidics provides the possibility to enhance the electrochemical performance, but its virtual interface is lack of development. This work demonstrates a dual electrolyte microfluidic reactor (DEMR) that improves the thermodynamic property and raises the electrochemical performance based on a laminar flow membrane-less architecture. Freed from hindrances of membrane structure and thermodynamic limitation, DEMR could bring in 6 times higher reactivity and draws electrode potentials closer to the equilibrium status (corresponding to less electrode overpotentials). The cathode potential was reduced from -2.1V to -0.82V and the anode potential dropped from 1.7V to 1V. During the conversion of CO<sub>2</sub>, the peak Faradaic and energetic efficiencies were recorded as high as 95.6% at 143 mA/cm<sup>2</sup> and 48.5% at 62 mA/cm<sup>2</sup>, respectively, and hence, facilitating future potential for larger-scale applications.

24

25 **Keywords**

26 CO<sub>2</sub> utilization

27 Energy storage

28 Electrochemistry

29 Dual electrolyte

30 Microfluidics

31

32 **1. Introduction**

33 Issues related to carbon dioxide (CO<sub>2</sub>) emission become increasingly important. Instead of CO<sub>2</sub>  
34 capture and sequestration, electrochemical conversion of CO<sub>2</sub> into usable fuels is an important  
35 option to provide a solution towards a carbon-neutral energy conversion.

36 Many research efforts on electrochemical reduction of CO<sub>2</sub>, and specifically on the  
37 development of electrode materials, have focused on increasing the reactivity and reducing the  
38 overpotential for a higher Faradaic efficiency. Various noble metal-based catalysts and different  
39 compositions have been tested with low electrical resistances in a three-electrode system[1, 2]  
40 and the synthesis of catalysts have demonstrated high turnover numbers as high as 350 h<sup>-1</sup>[3].  
41 Studies on catalyst structures, especially gas diffusion layers (GDLs), have been conducted to  
42 enhance the three-phase interaction and hence a larger active site area[4, 5]. The implementation  
43 of a gas diffusion electrode (GDE) with high porosity and specific surface in a DEMR help  
44 relieve the constraint from the effective electrolyte conductivity and electro-active site thickness  
45 limitations. In general, an electrode of an electrolytic cell comprises a substrate and a catalyst  
46 layer (CL), serving multiple functions in electrochemical reduction of CO<sub>2</sub> to formic acid, such

47 as absorbing gaseous CO<sub>2</sub>, transporting CO<sub>2</sub> from substrate to the CL, providing an active  
48 reaction site for catalyst(s) adhered on its surface, deliver formic acid from the CL into the  
49 electrolyte, and conducting protons and electrons with low resistance. At early stage, substantial  
50 attempts on developing electrodes with planar and mesh structures[6] were conducted, but  
51 outcomes were mostly unsatisfactory. GDEs, which create effective three-phase interfaces for  
52 gaseous reactants, electrodes and electrolytes, have been developed rapidly and are regarded as  
53 an effective solution towards low gaseous feed transfer rate and poor cell performance[7, 8]. A  
54 GDE usually comprises of a conventional catalyst layer, where carbon black is usually utilized to  
55 support catalyst particles, and a GDL[9]. GDL is usually made from porous materials and dense  
56 array of carbon fibers, whose high surface area would facilitate CO<sub>2</sub> transport and reduction.  
57 Two common examples are non-woven carbon paper and woven fabric carbon cloth, enhancing  
58 the interfacial area within the material of the electrode and the three-phase boundary. In addition  
59 to providing mechanical support and protection from corrosion or erosion, GDEs also perform  
60 other multiple roles including the pathway of CO<sub>2</sub> and electrolyte diffusion, intermediate of  
61 proton and electron transfer, passage for by-product removal for the purpose of preventing  
62 cathode flooding, medium of heat transfer. Studies of GDEs on CO<sub>2</sub> to formic acid conversion  
63 cell have been conducted by many researchers. Experiment with Pb-coated GDEs shows high  
64 reaction rate, high current density, high Faradaic efficiency ( $\approx 95\%$ ) and reasonable applied  
65 potential[10]. Another high performance catalyst, Ru-Pd alloy particles, has been incorporated  
66 with GDEs[11] too, whose competitiveness was revealed by 90% current efficiency at -1.1 V vs.  
67 SCE and 80 mA/cm<sup>2</sup>. Cu- and Zn- phthalocyanines have been coated and tested on GDEs,  
68 yielding formic acid at high current densities (100 mA/cm<sup>2</sup>)[12]. The issue related to CO<sub>2</sub>

69 solubility could also be relieved by GDE as the gaseous reactant molecules would diffuse  
70 through the porous reactive site with large geometric contact area[13].

71 More recently, multi-walled nanotubes and cobalt tetra-amino phthalocyanine composite  
72 modified electrodes were reported in literatures to further boost the catalysis process in terms of  
73 reactivity. Besides, the possibility of implementing ionic liquids[14-17] and organic  
74 electrolytes[18] [19, 20] as co-catalysts have been demonstrated to be able to improve the  
75 electrochemical performance and suppress side reactions. Although the above-mentioned  
76 methods have achieved slight catalyst degradations and low kinetic losses, electrode potentials  
77 have remained high and electrochemical reduction of CO<sub>2</sub> can hardly leap forward due to the  
78 thermodynamic limitation.

79 The aim of breaking the thermodynamic barrier has motivated a pH differential technique. It  
80 was reported that the overall cell and individual electrode potentials could be altered for better  
81 electrochemical performance by adjusting electrolyte pH conditions[21]. Although some  
82 researchers, including our group, have implemented this strategy in fuel cells and flow batteries  
83 with raised open-circuited voltages (OCV) and peak power densities[22], its application to  
84 electrolysis process, such as CO<sub>2</sub> electrochemical reduction, remains unexplored. A pH above 6  
85 would affect the intrinsic kinetics of CO<sub>2</sub> to formic acid conversion because of the limited CO<sub>2</sub>  
86 mass transfer rate. pH would also alter the forms of products and high concentration of formic  
87 acid would not be formed in case of neutral or base condition ( $pK_a = 3.8$  at 298 K)[23].

88 Theoretically, electrolyte pH adjustment would significantly lower electrode potentials and  
89 benefit CO<sub>2</sub> reduction by pairing the cathode with acid and the anode with alkaline electrolytes.  
90 Yet, most electrochemical reactors have been designed and developed based on polymer  
91 membrane structure[24, 25], which suffers from high cost, low interphase contact area, flooding

92 problem, and poor durability as an acid-alkaline separator. More recently, a state-of-the-art  
93 concept of microfluidic reactor has been reported[26, 27], using laminar electrolyte streams with  
94 distinctive behaviors to separate the cathode and anode. Microfluidics offers a virtual but  
95 effective layer to replace the conventional membrane, providing an ultimate solution towards  
96 some of the limitations of macroscale devices. Microfluidic electrochemical reactors soon spread  
97 widely in various applications such as quantitative detection of biological indicators[28, 29],  
98 synthesis of oxidation products[30], and wastewater treatment[31].

99 More specifically, researchers have shown the power of microfluidics to enhance the  
100 performance of CO<sub>2</sub> electrochemical reduction systems. By employing the microfluidic  
101 electrolyte flow, the water management issues at the electrode and membrane was eliminated.  
102 Additionally, continuous flow operation and individual electrode analysis becomes possible,  
103 making microfluidics an ideal electrochemical analysis platform. Multiple purposes were also  
104 well developed, including CO<sub>2</sub> sequestration[32], synthesis of gaseous fuels[33], CO<sub>2</sub> dissolution  
105 in physical solvents[34], and numerical analysis on intrinsic electrochemistry[35].

106 Despite these noticeable merits and achievements, breakthroughs of microfluidics on the  
107 electrochemical conversion of CO<sub>2</sub> to fuels could barely be found and it appears that the virtual  
108 layer is the key to facilitate further advancement. Microfluidics enables the operation conditions  
109 (e.g. electrolyte composition and pH) in a more flexible manner. The study by Whipple et al. [36]  
110 tested several electro-catalysts and the effects of electrolyte pH on the cell efficiency, revealing  
111 that cell operating at pH = 4 resulted in a significant improvement of cell performance, i.e.  
112 Faradaic and energetic efficiencies could achieve 89 and 45%, respectively, at current density of  
113 100 mA cm<sup>-2</sup>. These results pointed to the possibility that the thermodynamic constrains could be  
114 eliminated to some extent by microfluidics, because the membraneless nature could realize

115 individual tailoring of the composition of the anolyte and catholyte, thus allowing the kinetics  
116 and thermodynamic at the anode and cathode to be independently optimized[37]. Usually, in a  
117 membrane-based electrochemical system, the cell would be operated either on under acidic or  
118 alkaline media. In a microfluidic reactor, on the other hand, mixed-media operation could be  
119 achievable regardless of the membrane stability, i.e. one electrode in acidic media and another in  
120 alkaline conditions. Certain combinations of anode and cathode stream composition will result in  
121 very low on-set voltages, while other combinations may lead to high potentials as a result of the  
122 pH dependence of standard electrode potentials, which would be respectively favorable for CO<sub>2</sub>  
123 electrochemical reduction [37].

124 Accordingly, we report a dual electrolyte microfluidic reactor (DEMR) converting CO<sub>2</sub> into  
125 formic acid. Formic acid is selected as the target product because of its role as a common energy  
126 storage medium[38-40] and commercialization prospect[41, 42]. To optimize the reactor  
127 performance, our research covers electrode material selection, catalyst preparation, and pH  
128 optimization for anolyte and catholyte. By breaking the thermodynamic barrier, both reactivity  
129 and Faradaic efficiency of the system are enhanced, revealing a new solution towards greenhouse  
130 gas mitigation and energy storage shortage issues.

131

132

## 133 **2. Methodology**

### 134 **2.1 Thermodynamic design**

135 The major reactions under dual electrolyte arrangement in our DEMR are provided in Eq. 1, 2  
136 and 3.

137 Cathode reaction (acid):



140 Anode reaction (alkaline):



142 The equilibrium potentials of the cathode reaction,  $E_{\text{cathode}}$ , can be calculated from Eq. 4  
 143 based on Nernst equation[43]:

144 
$$E_{\text{cathode}} = E_{\text{cathode @ pH=0}}^0 - \frac{RT}{2F} \cdot \ln\left(\frac{1 + \frac{K_1}{[\text{H}^+]} \cdot (1 + \frac{K_2}{[\text{H}^+]})}{1 + \frac{K_3}{[\text{H}^+]}} \cdot \frac{1}{[\text{H}^+]^2}\right)$$
 (4)

145 where

146 R: the universal gas constant  $8.314 \text{ JK}^{-1}\text{mol}^{-1}$ ,

147 T: temperature (298K),

148 F: Faraday constant ( $96485 \text{ Cmol}^{-1}$ ),

149  $K_1$ : the equilibrium constant between  $\text{CO}_2$  and  $\text{HCO}_3^-$  ( $K_1 = e^{-\text{p}K_1} = e^{-6.39}$ )[43],

150  $K_2$ : the equilibrium constant between  $\text{CO}_2$  and  $\text{CO}_3^{2-}$  ( $K_2 = e^{-\text{p}K_2} = e^{-10.32}$ )[43],

151  $K_3$ : the equilibrium constant between  $\text{CO}_2$  and  $\text{HCOOH}$  ( $K_3 = e^{-\text{p}K_3} = e^{-3.75}$ )[43],

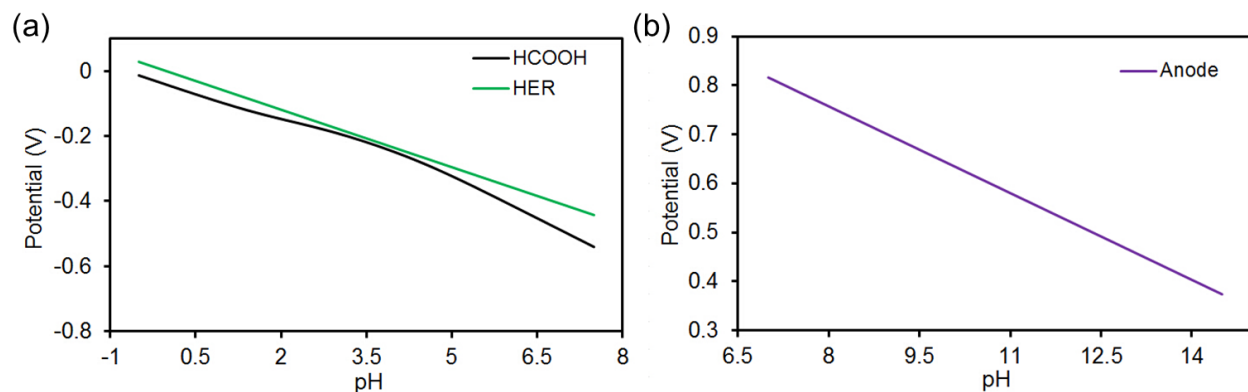
152  $K_i = e^{-\text{p}K_i}$ ,

153  $E_{\text{cathode @ pH=0}}^0$ : standard electrode potential at pH=0 recorded in 10 mM formate and 10  
 154 mM  $\text{CO}_2$  at 310K (-0.042V)[43],

155  $[\text{H}^+] = 10^{-\text{pH}}$ .

156 Fig. 1 shows the Pourbaix diagrams of three dominant reactions in a  $\text{CO}_2$  reduction system, i.e.  
 157  $\text{CO}_2$  to formic acid reaction, undesirable hydrogen evolution reaction (HER), and anode oxygen  
 158 evolution reaction. Corresponding Nernst potentials of each reactions are plotted against pH  
 159 values[44]. As can be observed, the individual potentials of the oxygen and hydrogen electrodes

160 drop linearly with elevated pHs, whereas the CO<sub>2</sub> reduction potentials would be reduced at  
161 lowered pHs, demonstrating the thermodynamic foundation of a DEMR.



162  
163 Fig. 1. Pourbaix diagrams of (a) CO<sub>2</sub> to HCOOH conversion (cathode reaction) and HER; and (b)  
164 oxygen evolution reaction (anode reaction).

## 165 2.2 Catalyst preparation

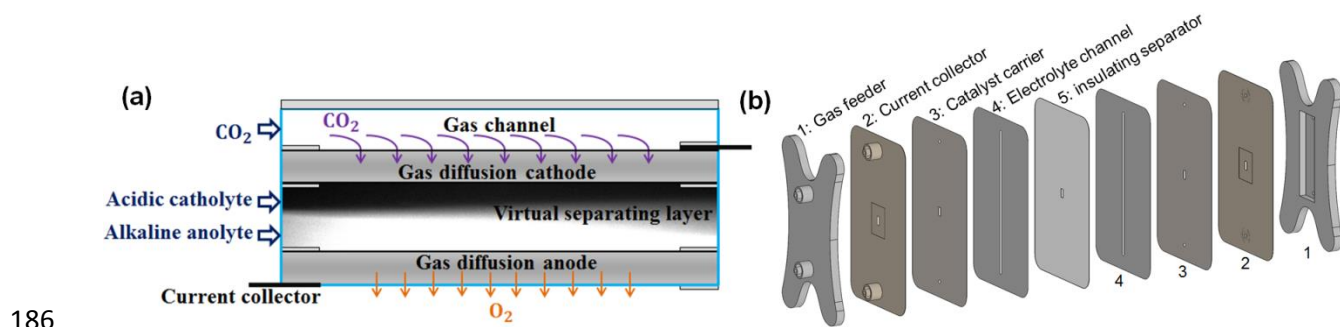
166 Commercially available catalysts (Johnson Matthey) supported by carbon paper were used as  
167 electrodes and Nafion (DuPont) solution was used as the catalyst binder. Different types of  
168 catalysts (i.e. Pd, PtRu, PtIr, Sn, Pt black, Pb) were used as mentioned in the catalyst selection  
169 section. Catalyst inks were prepared by sonicating mixtures of 28 mg catalyst, 126  $\mu$ L of 10 wt %  
170 Nafion solution to achieve 30:1 catalyst to Nafion ratio, and 2800  $\mu$ L of isopropyl alcohol for 1 h.  
171 The ink was then scattered onto a PTFE-hydrophobized gas diffusion carbon paper (HCP120,  
172 Hesentel) with sizes 2.5 cm (L)  $\times$  1.1 cm (W) by spray gun. Measuring the net weight increase of  
173 carbon paper before and after spraying, the catalyst loading on the electrodes was 5 mg/cm<sup>2</sup>.

## 174 2.3 Cell fabrication

175 The electrodes were housed between two 0.05-cm-thick Poly(vinyl chloride) (PVC) sheets as  
176 embedding plates. Two silver plates were used as current collectors. Each of the embedding  
177 plates were machined with a 0.2 cm (W)  $\times$  0.5 cm (L) window as reaction area. Two 0.01-cm-



178 thick PVC sheets were used to separate the electrodes and create identical anolyte and catholyte  
 179 channels of 0.2 cm (W) × 7.5 cm (L), between which another 0.01-cm-thick PVC sheet with a  
 180 0.2 cm (W) × 0.5 cm (L) window was sandwiched in-between, indicated as ‘insulating separator’  
 181 in Fig. 2. The insulating separator is used to form the catholyte and anolyte interactive and  
 182 contact area. A 5 cm (L) × 1 cm (W) × 0.5 cm (H) chamber was machined to act as the CO<sub>2</sub>  
 183 reservoir for the cathode side. All layered components were fabricated using CO<sub>2</sub> laser ablation  
 184 system (VLS 2.30, Universal Laser System) and clamped together by binder clips (Highmark), as  
 185 shown in Fig. 2.



186  
 187 Fig. 2. Demonstration of the microfluidic reactor. (a) Schematic diagram of a DEMR; and (b)  
 188 Component configuration (N.B. the virtual separating layer is identified by fluorescein  
 189 microscopy).

## 190 2.4 Electrochemistry

191 Electrochemical tests were conducted by holding the cell at constant potentials by an  
 192 electrochemical station (CHI600E, CHInstruments, Inc) with a sampling frequency of 250 Hz.  
 193 The measurement and record of each data point took a total of 200 seconds. The first 100  
 194 seconds was the stabilizing phase, followed by the 100-second steady state. Each data point was  
 195 collected by averaging the integration of the 100-second steady-state current data to eliminate  
 196 transient artifacts. Controlled by a mass flow controller (GFC17, Aalborg), gaseous CO<sub>2</sub> (≥ 99.5%

197 purity, Linde) was fed into the cathode chamber at a flow rate of 80 mL/min and migrated  
198 through the GDLs to the catalyst surfaces. Electrolytes stored in syringe tubes were driven by  
199 syringe pumps (LSP02-1B, Longer Pump) at a flow rate of 500  $\mu\text{L}/\text{min}$  and continuously guided  
200 through the microchannels by plastic tubes. The electrolytes were not recirculated and the syringe  
201 tubes were refilled upon electrolyte depletion to restart the experiment. Individual potentials of  
202 anode and cathode were recorded with digital multi-meters (Fluke) connected between each  
203 electrode and an external Ag/AgCl reference electrode in the exit electrolyte stream. Current and  
204 power densities were calculated using the exposed surface area of the electrodes (i.e.  $0.1\text{ cm}^2$ ).

205 In terms of the cations/anions selection, there exists an inter-conversion amongst  $\text{CO}_3^{2-}$ ,  
206  $\text{HCO}_3^-$  and  $\text{CO}_2(\text{aq})$ [45-47], where high concentration of  $\text{CO}_3^{2-}$  would be beneficial to the  
207 chemical kinetics of the  $\text{HCO}_3^-$  evolution but lower the selectivity of formic acid generation[23].  
208 Under slight base condition, the reaction:  $\text{HCO}_3^- + \text{OH}^- \rightarrow \text{CO}_3^{2-} + \text{H}_2\text{O}$  would decrease the  
209 pH and hence deplete  $\text{CO}_2(\text{aq})$  as well. Because of the complexity with respect to the inter-  
210 conversion and the fact that other anions, such as  $\text{Cl}^-$  and  $\text{Br}^-$ , would bring in the risk of  
211 electrolysis towards poisonous oxidants,  $\text{SO}_4^{2-}$  is used in this study. It should also be noted that  
212  $\text{K}^+$  was selected as the cation because the cathode potential of formic acid generation reaction  
213 would be shifted to thermodynamic superiority over HER. Cations such as  $\text{Na}^+$  and  $\text{Li}^+$  were also  
214 found to have similar effect, but less significant compared with  $\text{K}^+$ .

## 215 **2.5 Formic acid determination method**

216 The determination of formic acid adopted the method proposed by Sleat et al. [48], which was  
217 based on a non-enzymatic specific reaction forming a red color with an absorption maximum at  
218 510 nm when formate and several chemicals were mixed. During each set of experiment, exit  
219 electrolyte streams were collected after reaching steady state, 0.25 mL of which was extracted

220 and diluted by 0.25 mL deionized water as the sample. Meanwhile, 0.05 g citric acid was mixed  
221 with 1 g acetamide followed by ultrasonic dispersion in 10 mL 2-propanol. 0.5 mL of this  
222 mixture, together with 0.5 mL of the sample were dissolved in a mixture of 0.025mL 30% w/v  
223 sodium acetate and 1.75mL acetic anhydride for 1.5 hr. The absorbance of the solution mixture  
224 was obtained by a spectrophotometer (6105 U.V./Vis. Jenway) to determine the formate  
225 concentration. Calibration was conducted by quantitatively determining corresponding color  
226 formation in the presence of formate at 2.5, 5, 7.5, 10, 12.5, 15, 17.5 and 20 mmol/L, giving an  
227 correlative equation in Eq. 5.

$$228 \quad 0.0588 \times \text{Concentration of HCOO}^- + 0.0562 = \text{Absorbance} \quad (5)$$

## 229 **2.6 Efficiency calculation**

230 Faradaic and energetic efficiencies are two key benchmarks for a CO<sub>2</sub> electrochemical reduction  
231 system. Faradaic efficiency indicates the fraction of the transferred electrons to facilitate the  
232 desired electrochemical reaction in a system. In this study, it is the formic acid formation  
233 reaction. Energetic efficiency is to measure the portion of energy converted and stored formic  
234 acid.

235 In order to calculate the Faradaic efficiency, we could obtain the total electrons passing  
236 through the reaction sites by measured current, then determine the electrons used for generating  
237 desired products based on the detected amount of formic acid. Denote the flow rate as M  $\mu\text{L}/\text{min}$   
238 and the applied current to be N ampere. Assume that HCOO<sup>-</sup> concentration is Y mol/L. The  
239 amount of detectable HCOO<sup>-</sup> is  $Y \times \frac{M}{10^6 \times 60}$  mol/s; hence, the amount of electrons transferred to  
240 produce formic acid is  $2 \times Y \times \frac{M}{10^6 \times 60}$  mol/s. On the other hand, the number of electrons  
241 delivered to the electrode is  $N \times 1.04 \times 10^{-5}$  mol/s, giving Faradaic efficiency as shown in Eq.  
242 6.

243 
$$FE = \frac{2 \times Y \times \frac{M}{10^6 \times 60}}{N \times 1.04 \times 10^{-5}} \times 100\% \quad (6)$$

244 As for energetic efficiency, which considers voltage losses, the determination equation is  
245 defined in Eq. 7.

246 
$$\text{Energetic efficiency} = \frac{\text{Standard potential}}{\text{Standard potential} + \text{Overpotential}} \times \text{Faradaic efficiency} \quad (7)$$

247

### 248 **3. Results and discussion**

#### 249 **3.1 Cathode catalyst selection**

250 Pourbaix diagrams in Fig. 1 show the thermodynamic advantage of HER over formic acid  
251 generation. Experimentally, the applied cathode potentials for kinetically slow formic acid  
252 generation reaction, i.e. Reaction (1), would be from  $\sim -0.8\text{V}$  to  $-1.8\text{V}$  with the overpotential from  
253  $\sim -0.4\text{V}$  to  $-1.4\text{V}$ [49], which is in the same potential range of HER, leading to selectivity decrease  
254 in aqueous electrolytes[13]. Thus, researchers have put efforts to select catalysts with high  
255 hydrogen overpotential to suppress HER, including Hg, In, Pb, and Sn[23, 50].

256 A DEMR was fabricated to construct a microchannel network, based on which different  
257 catalysts were tested for the comparison of key parameters such as current density, Faradaic  
258 efficiency and energy efficiency. Using the same electrolyte, i.e. 0.5 mol/L aqueous  $\text{K}_2\text{SO}_4$   
259 solution at pH=7, and anode material, i.e. commercially available PtRu (1:1 at.%) [51], cathode  
260 catalyst materials including palladium[52], tin[53], lead[10] and platinum series were tested for  
261 comparison.

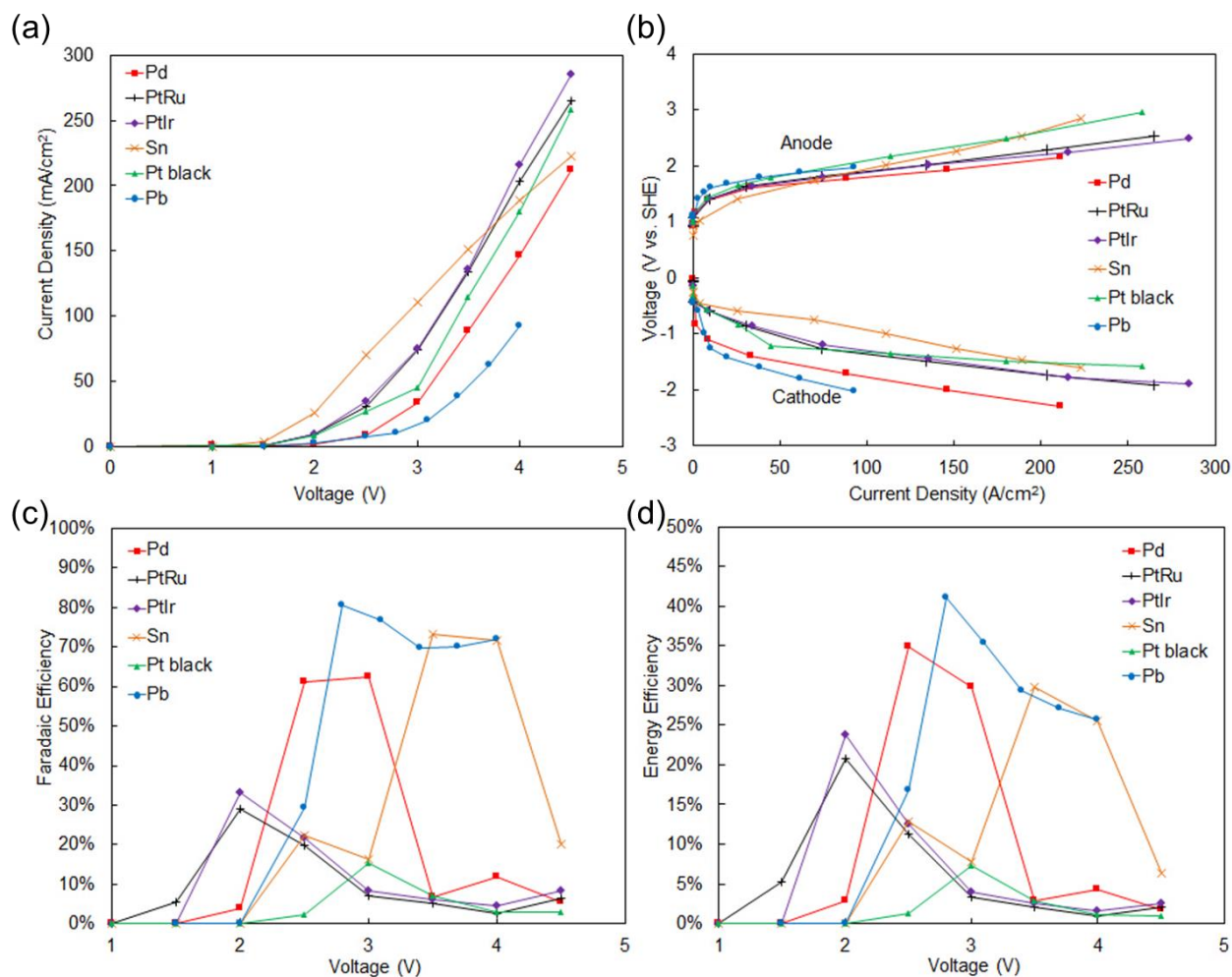
262 Different current densities were applied to the reactor by varying the voltages to obtain the  
263 trends of reactivity and efficiencies.  $\text{CO}_2$  concentration polarization would lead to lower Faradaic  
264 efficiency with increase in the applied voltage, so does the energetic efficiency because of the  
265 superposition of the elevated overpotentials. Nevertheless, there were dissents that on Sn[54] and

266 Pb at a CO<sub>2</sub> pressure of 5000 kPa(abs) [55], parabolic dependence of Faradaic efficiency on  
267 current density could be observed. These contradictions may be due to the rate determining step  
268 in the intrinsic kinetics of the formic acid generation reaction and should be addressed in a  
269 microfluidic reactor.

270 As shown in Fig. 3a, at a controlled voltage, PtIr showed the highest current densities,  
271 followed by PtRu, Pt black, and Pd. Sn catalyst demonstrated the highest current density below  
272 3.5V and the smallest on-set electrolysis voltage. Pb showed the lowest current density.  
273 Microfluidics enables the investigation on the polarization of each electrodes as they were well  
274 separated by the virtual mixing layer. It could be observed that the ranking of whole cell  
275 performance conformed to that of the individual electrodes. The electrocatalytic activity toward  
276 CO<sub>2</sub> reduction could be further improved via tuning the morphology, electronic structure, and  
277 electrolysis conditions[56, 57], as the reactivity is highly dependent on the balance between the  
278 interactive strength (between CO<sub>2</sub><sup>-</sup> and the nanoscale metal surface) and the kinetics of  
279 following electronation and desorption from the electrode surface.

280 However, when looking at Faradaic efficiency, which indicates the portion of electrons used  
281 for producing formic acid, Pt-series catalysts, although with high catalytic reactivity, showed <  
282 35% Faradaic efficiency, i.e. low selectivity of converting CO<sub>2</sub> towards formic acid. This is due  
283 to the high water electrolysis catalytic rate and low hydrogen overpotential of Pt, favoring the  
284 HER[58, 59]. Although modifying the symmetry of the surface and introducing densely packed  
285 kink atoms along step lines would boost the activity for CO<sub>2</sub> reduction, the dominant reaction on  
286 Pt is to reduce CO<sub>2</sub> to CO[60], which might be adsorbed onto the catalyst surface, causing  
287 blockage.

288 Pb demonstrated a peak Faradaic efficiency as high as 80.5% at 2.8V, followed by Sn (73.2%  
 289 at 3.5V) and Pd (62.4% at 3V). In terms of energetic efficiency, which takes voltage losses into  
 290 consideration[61], Pb still showed superior performance up to 41% and surpassed other catalysts,  
 291 implying its lower voltage loss. Selectivity is the key parameter to evaluate a CO<sub>2</sub>  
 292 electrochemical reduction system and the purity of produced formic acid, and hence it should be  
 293 considered prior to reactivity. Therefore, Pb was chosen as the cathode catalyst.



294  
 295 Fig. 3. (a) Polarization curves, (b) the corresponding individual electrode polarization curves, (c)  
 296 Faradaic efficiencies, and (d) energetic efficiencies for cathode catalyst materials including Pd,  
 297 PtRu, PtIr, Sn, Pt black and Pb. Anode catalyst material was PtRu. Both catholyte and anolyte  
 298 were kept at pH=7 with a flow rate of 0.5 mL/min. CO<sub>2</sub> supply rate is 50 sccm.

### 3.2 Catholyte pH optimization

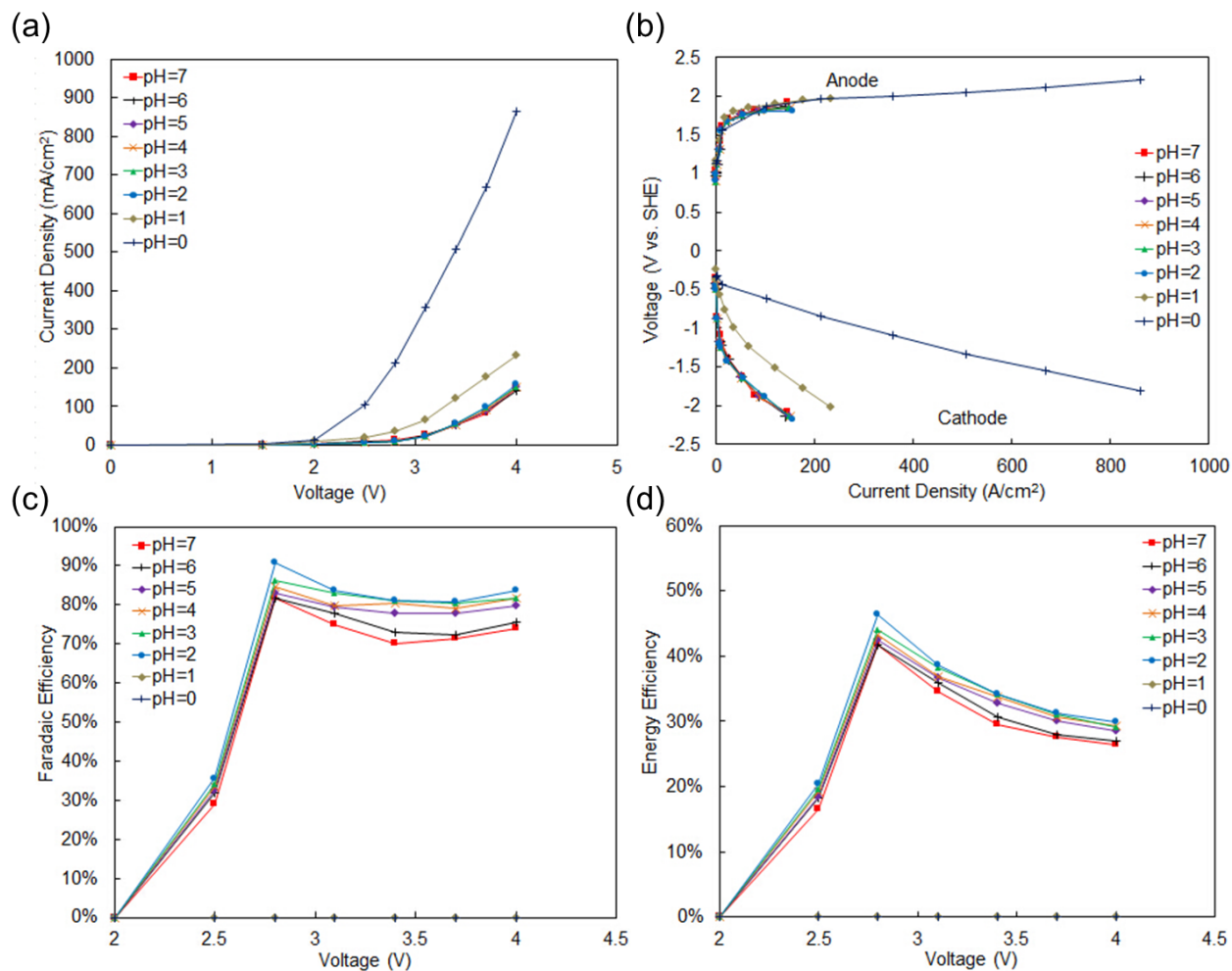
As previously explained, pH is an important factor that affects the performance of the DEMR. To identify the optimal catholyte pH, we applied the control variate method based on Pb cathode and PtRu anode combination. The anolyte pH was kept constant at pH=7, using common aqueous 0.5 mol/L K<sub>2</sub>SO<sub>4</sub> solution, while the catholytes at different pHs were prepared by adjusting 0.5 mol/L K<sub>2</sub>SO<sub>4</sub> with 0.5 mol/L H<sub>2</sub>SO<sub>4</sub>. This preparation process could help preclude the effect of conductivity and focus on pH. The reason to keep the conductivity constant is that a catholyte conductivity below 10 S/m would influence the applied reactor voltage and potential distribution in the electrode, which could be more significant with increasing the electrode thickness and current density[23]. To ensure a univariate analysis, sulfuric acid is used as the pH adjustor upon the potassium sulphate solution.

As can be seen in Fig. 4a, quantitated by current density, the whole cell reactivity at pH=0 catholyte was five times as much as that of pH=1, whose reactivity was more than twice as much as those of pH=2. The phenomenon corresponded to the fact that the concentration of H<sup>+</sup> dropped significantly from 1 mol/L to 0.1 mol/L. From pH=2 onwards, slight degradation of reactivity was observed because the absolute pH difference was less than 0.01 mol/L.

Fig. 4b gave a more detailed look into individual electrode performance. The individual anode polarization curves highly fitted with each other, whilst the cathode polarization curves followed the trend of the whole cell reactivity, i.e. cathode reactivity at pH=0 preceded pH=1 and stabilized from pH=2. The distinguished individual electrode reactivity validated the good utilization of microfluidic network by DEMR without significant mass transport loss.

In terms of efficiencies, no formic acid was detected in pH=0 and 1 due to the fact that hydrogen evolution reaction dominated at such high H<sup>+</sup> concentration and a large amount of

322 gaseous by-products could be observed during the reaction. The situation changed at pH=2,  
 323 where a Faradaic efficiency of 90.8% and energetic efficiency of 46.4% was obtained at 2.8V.  
 324 From pH=3 onwards, the figures were gradually diminishing, which was attributed to the drop in  
 325 H<sup>+</sup> concentration. Considering both reactivity and efficiency, pH=2 gave the optimal overall  
 326 performance and hence was selected as catholyte condition of our DEMR for further study.



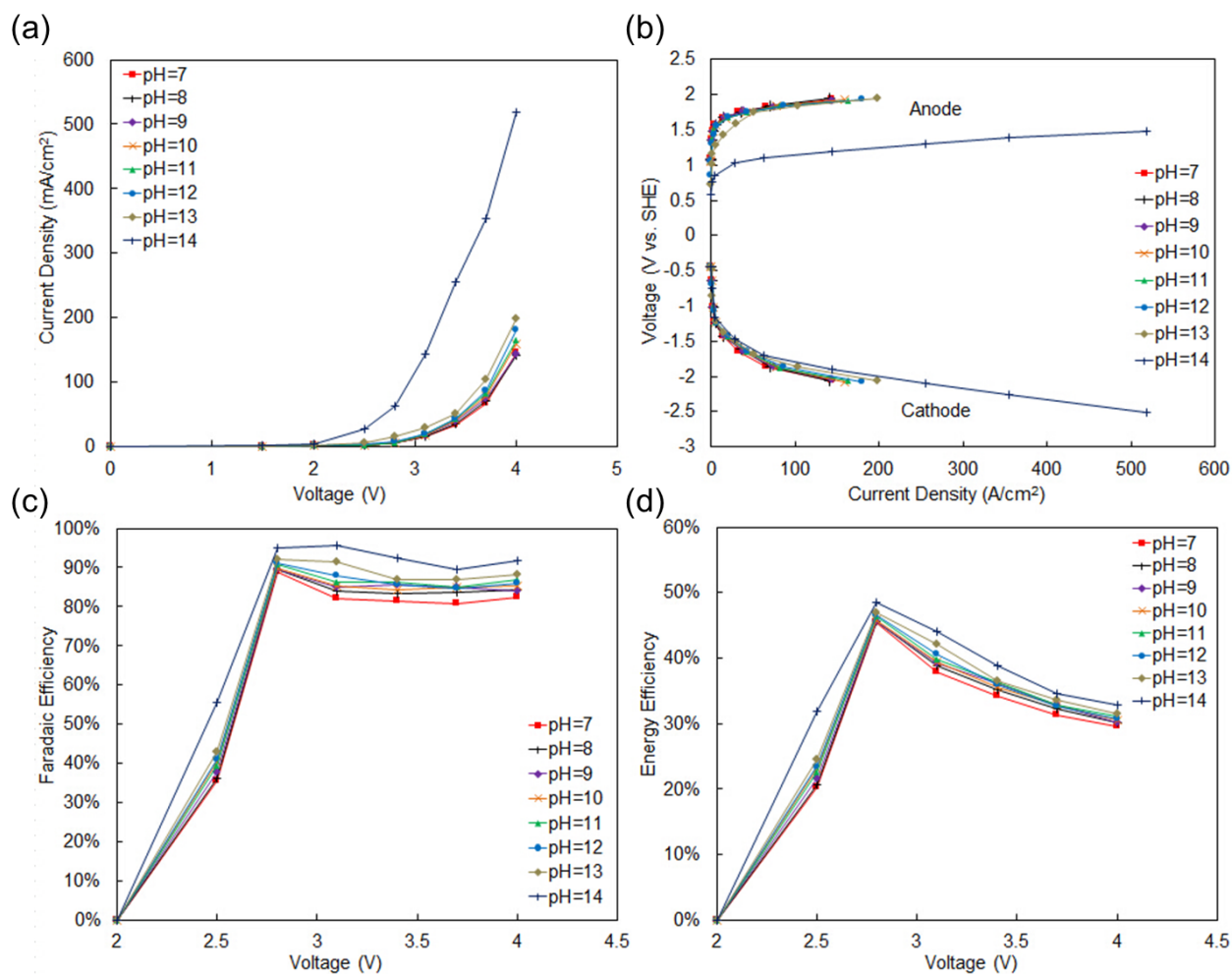
327  
 328 Fig. 4. (a) Polarization curves, (b) the corresponding individual electrode polarization curves, (c)  
 329 Faradaic efficiencies, and (d) energetic efficiencies. Cathode catalyst material was Pb and anode  
 330 was PtRu. Catholyte pH ranged from 7 to 0 and anolyte was kept at pH=7 with a flow rate of 0.5  
 331 mL/min. CO<sub>2</sub> supply rate is 50 sccm.

### 332 3.3 Anolyte pH optimization



333 With catholyte pH set to 2 (Section 3.2), the effect of anolyte pH was studied from pH=7 to  
334 pH=14, where the latter showed overwhelming advantage over others in terms of reactivity, i.e.  
335 four times more than pH=13 as quantitated by current density (Fig. 5a). Individual electrode  
336 polarization curves (Fig. 5b) demonstrated that pH=14 improved anode performance, which did  
337 not affect the cathode side and hence corroborating again that the microfluidics in our DEMR  
338 could effectively separate electrolytes and create distinguished conditions for electrodes.

339 Efficiencies were found in accordance with reactivity. When anolyte pH was 14, the peak  
340 Faradaic efficiency and energetic efficiency were as high as 95.6% and 48.5%, respectively.  
341 With decreasing pH, efficiencies dropped as indicated in Fig. 5c and 5d. It should be noted that  
342 increasing further the pH would lead to catalyst poisoning and instability. Thus, pH=14 was  
343 selected as anolyte pH for our DEMR.



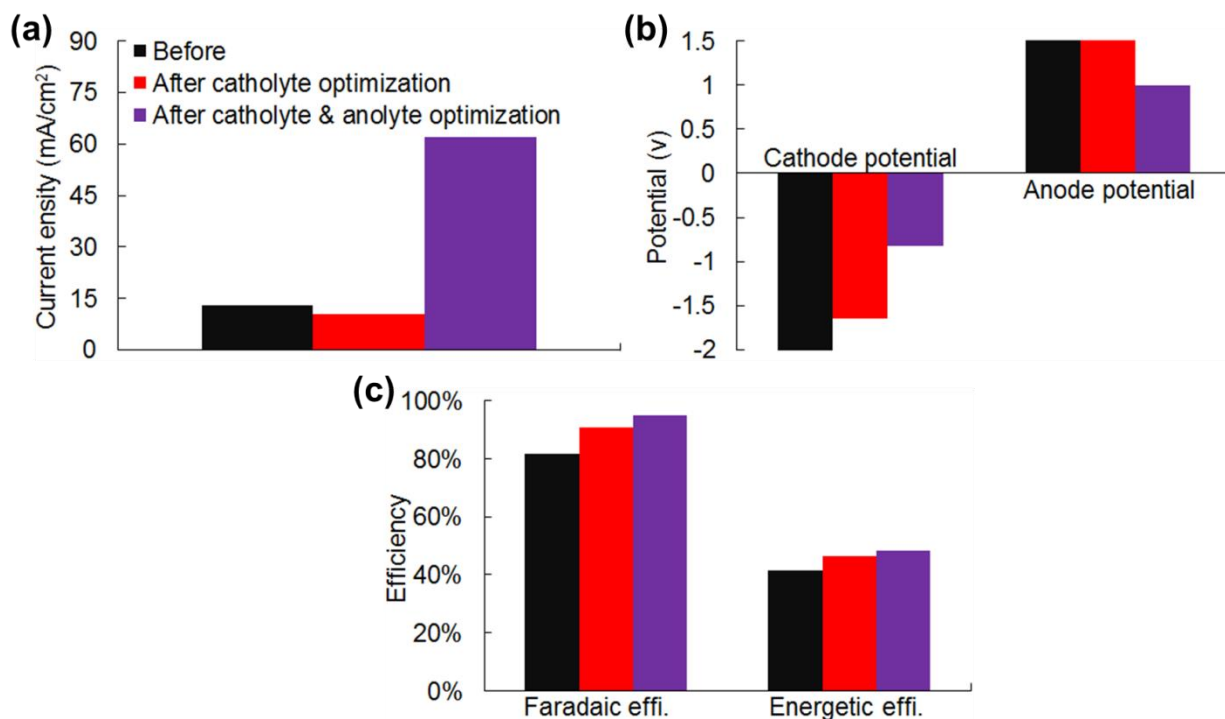
344

345 Fig. 5. (a) Polarization curves, (b) the corresponding individual electrode polarization curves, (c)  
 346 Faradaic efficiencies, and (d) energetic efficiencies. Cathode catalyst material was Pb and anode  
 347 was PtRu. Catholyte was kept at pH=2 and anolyte pH ranged from 7 to 14 with a flow rate of  
 348 0.5 mL/min. CO<sub>2</sub> supply rate is 50 sccm.

### 349 3.4 Optimization comparison and discussion

350 Fig. 6 summarizes the improvement introduced by the pH optimization. The current density  
 351 remained almost unchanged after catholyte optimization because of the slight pH change;  
 352 however, the current density was raised significantly from ~10 to ~60 mA/cm<sup>2</sup> after anolyte  
 353 optimization, as can be seen in Fig. 6a. Fig. 6b demonstrates the thermodynamic improvement,  
 354 where the cathode potential was reduced from -2.1V to -0.82V and the anode potential dropped

355 from 1.7V to 1V. Most importantly, Fig. 6c shows the increase of efficiencies, where electrolyte  
 356 pH optimization raised the peak Faradaic efficiency from 81.6% to 95.6% and the peak energetic  
 357 efficiency from 41.7% to 48.5%.



358  
 359 Fig. 6. (a) Current densities at an applied voltage of 2.8V, (b) cathode potentials at 100 mA/cm<sup>2</sup>  
 360 under catholyte pHs of 7, 1 and 0; anode potentials at 150 mA/cm<sup>2</sup> under anolyte pHs of 7, 13  
 361 and 14, and (c) peak Faradaic and energetic efficiencies, before and after electrolyte optimization.

362 In theory, acid conditions on the cathode side and alkaline on the anode side can  
 363 thermodynamically lower the potential difference. When applying acidic catholyte, a lower  
 364 equilibrium potential of cathode reaction can be obtained (-0.199V in acid vs. -1.02V in alkaline,  
 365 vs. NHE). More desired product, formic acid, can be generated with lower pH, especially when  
 366 pH is less than 3[62], and hence increasing the Faradaic efficiency. Lower pH also favors the  
 367 current density enhancement by reducing polarization losses, i.e. improves the reaction kinetics.  
 368 It should be noted that unwanted HCO<sub>3</sub><sup>-</sup> or HCO<sub>3</sub><sup>2-</sup> could be generated under neutral or alkaline

369 conditions and the reactive  $\text{CO}_2(\text{aq})$  would be sequestered as bicarbonate/carbonate at  $\text{pH} > 9$ .  
370 On the anode side, alkaline environment ensures the oxygen formation at low equilibrium  
371 potential.

372 A virtual separating layer between catholyte and anolyte can be observed in Fig. 2a. Heat  
373 visualization[63] showed that acid-base interfacial heat is dominant in a DEMR, whose ohmic  
374 Joule heat is much less than a single electrolyte system. Acid-base neutralization is known as a  
375 superfast reaction with a rate constant  $\sim 10^{11} \text{ M}^{-1} \text{ s}^{-1}$ [64] and might lead to significant losses  
376 without proper control method. This problem has been investigated and addressed by our  
377 previous study[63], where the fluorescence microscopy was utilized to demonstrate that raising  
378 the flow rate (e.g. 1.4 mL/min) could enhance the heat removal and formed a thinner interfacial  
379 mixing layer, hence controlling the reactor temperature and suppressing the heat loss.

380 Despite the fact that a microfluidic network can shorten the path required for ions diffusion in  
381 the narrow channel[65], the solubility of  $\text{CO}_2$  is rather low in aqueous electrolytes, limiting its  
382 mass transfer to the reaction site. Microfluidics properties in our DEMR can be enhanced by  
383 fully utilizing the large interfacial areas and effective three-phase interface (i.e. gaseous  $\text{CO}_2$ ,  
384 solid catalyst, and liquid electrolyte) in gas diffusion electrodes[66]. Also, pH adjustment can be  
385 applied on other electrolytes with high  $\text{CO}_2$  solubility and HER overpotential, such as organic  
386 electrolytes[18] [19, 20] and ionic liquids[67-69], to improve the whole cell performance.

387

#### 388 **4. Conclusions**

389 This work demonstrates the possibility of advancing  $\text{CO}_2$  electrochemical reduction via  
390 thermodynamic approach based on microfluidics. Different catalysts favoured  $\text{CO}_2$  electro-  
391 conversion into formic acid to various extents. By comparing six commonly used noble metal

392 catalysts, the combination of Pb cathode and PtRu anode was found to give the highest  
393 efficiencies despite of its relatively low catalytic activity. The merit comes from the fact that Pb  
394 has higher overpotentials for HER[10] and Pt is an active oxygen evolution catalyst. This study  
395 is the first systematic investigation to apply pH differential technique on CO<sub>2</sub> reduction,  
396 concluding that catholyte pH=2 and anolyte pH=14 output the optimal cell performance. In a  
397 dual electrolyte system, the reactivity was tripled than a single neutral electrolyte arrangement  
398 and the peak Faradaic efficiency was improved from 81.6% to 95.6%. In conclusion, this design  
399 not only provides a solution towards the improvement of current CO<sub>2</sub> utilization system, but also  
400 serves as a potential powerful and efficient energy storage platform.

401

#### 402 **Acknowledgement**

403 This project is financially supported by the CRCG of the University of Hong Kong and the  
404 Scottish – Hong Kong SFC/RGC Joint Research Scheme XHKU710/14 and SFC Project  
405 H15009.

406

#### 407 **References**

- 408 [1] J. Qiao, Y. Liu, F. Hong, J. Zhang, A review of catalysts for the electroreduction of carbon  
409 dioxide to produce low-carbon fuels, *Chemical Society Reviews*, 43 (2014) 631-675.  
410 [2] J.P. Jones, G. Prakash, G.A. Olah, Electrochemical CO<sub>2</sub> reduction: recent advances and  
411 current trends, *Israel Journal of Chemistry*, 54 (2014) 1451-1466.  
412 [3] E.E. Benson, C.P. Kubiak, A.J. Sathrum, J.M. Smieja, Electrocatalytic and homogeneous  
413 approaches to conversion of CO<sub>2</sub> to liquid fuels, *Chemical Society Reviews*, 38 (2009) 89-99.  
414 [4] A.J. Martín, G.O. Larrazábal, J. Pérez-Ramírez, Towards sustainable fuels and chemicals  
415 through the electrochemical reduction of CO<sub>2</sub>: lessons from water electrolysis, *Green Chemistry*,  
416 17 (2015) 5114-5130.  
417 [5] S. Park, J.-W. Lee, B.N. Popov, A review of gas diffusion layer in PEM fuel cells: materials  
418 and designs, *international journal of hydrogen energy*, 37 (2012) 5850-5865.  
419 [6] Y. Hori, H. Wakebe, T. Tsukamoto, O. Koga, Electrocatalytic process of CO selectivity in  
420 electrochemical reduction of CO<sub>2</sub> at metal electrodes in aqueous media, *Electrochimica Acta*, 39  
421 (1994) 1833-1839.

422 [7] C. Simon, F. Hasché, D. Müller, H.A. Gasteiger, Influence of the Gas Diffusion Layer  
423 Compression on the Oxygen Mass Transport in PEM Fuel Cells, *ECS Transactions*, 69 (2015)  
424 1293-1302.

425 [8] G. Lu, H. Wang, Z.-Y. Bian, X. Liu, Electrocatalytic Reduction of CO<sub>2</sub> to Formic Acid on  
426 Palladium-Graphene Nanocomposites Gas-Diffusion Electrode, *Journal of nanoscience and*  
427 *nanotechnology*, 14 (2014) 7097-7103.

428 [9] H.-R.M. Jhong, S. Ma, P.J.A. Kenis, Electrochemical conversion of CO<sub>2</sub> to useful chemicals:  
429 current status, remaining challenges, and future opportunities, *Current Opinion in Chemical*  
430 *Engineering*, 2 (2013) 191-199.

431 [10] C.H. Lee, M.W. Kanan, Controlling H<sup>+</sup> vs CO<sub>2</sub> reduction selectivity on Pb electrodes, *ACS*  
432 *Catalysis*, 5 (2014) 465-469.

433 [11] N. Furuya, T. Yamazaki, M. Shibata, High performance Ru-Pd catalysts for CO<sub>2</sub> reduction  
434 at gas-diffusion electrodes, *Journal of Electroanalytical Chemistry*, 431 (1997) 39-41.

435 [12] M.N. Mahmood, D. Masheder, C.J. Harty, Use of gas-diffusion electrodes for high-rate  
436 electrochemical reduction of carbon dioxide. II. Reduction at metal phthalocyanine-impregnated  
437 electrodes, *Journal of Applied Electrochemistry*, 17 (1987) 1223-1227.

438 [13] D. Kopljár, A. Inan, P. Vindayer, N. Wagner, E. Klemm, Electrochemical reduction of CO<sub>2</sub>  
439 to formate at high current density using gas diffusion electrodes, *Journal of Applied*  
440 *Electrochemistry*, 44 (2014) 1107-1116.

441 [14] M. Alvarez-Guerra, J. Albo, E. Alvarez-Guerra, A. Irabien, Ionic liquids in the  
442 electrochemical valorisation of CO<sub>2</sub>, *Energy & Environmental Science*, 8 (2015) 2574-2599.

443 [15] D.R. MacFarlane, N. Tachikawa, M. Forsyth, J.M. Pringle, P.C. Howlett, G.D. Elliott, J.H.  
444 Davis, M. Watanabe, P. Simon, C.A. Angell, Energy applications of ionic liquids, *Energy &*  
445 *Environmental Science*, 7 (2014) 232-250.

446 [16] Z. Zhang, S. Hu, J. Song, W. Li, G. Yang, B. Han, Hydrogenation of CO<sub>2</sub> to Formic Acid  
447 Promoted by a Diamine-Functionalized Ionic Liquid, *ChemSusChem*, 2 (2009) 234-238.

448 [17] M.R. Thorson, K.I. Siil, P.J. Kenis, Effect of Cations on the Electrochemical Conversion of  
449 CO<sub>2</sub> to CO, *Journal of the Electrochemical Society*, 160 (2013) F69-F74.

450 [18] E. Rischbieter, A. Schumpe, V. Wunder, Gas solubilities in aqueous solutions of organic  
451 substances, *Journal of Chemical & Engineering Data*, 41 (1996) 809-812.

452 [19] D.-w. Yang, Q.-y. Li, F.-x. Shen, Q. Wang, L. Li, N. Song, Y.-n. Dai, J. Shi,  
453 Electrochemical Impedance Studies of CO<sub>2</sub> Reduction in Ionic Liquid/Organic Solvent  
454 Electrolyte on Au Electrode, *Electrochimica Acta*, 189 (2016) 32-37.

455 [20] R. Kortlever, J. Shen, K.J.P. Schouten, F. Calle-Vallejo, M.T. Koper, Catalysts and  
456 Reaction Pathways for the Electrochemical Reduction of Carbon Dioxide, *The journal of*  
457 *physical chemistry letters*, 6 (2015) 4073-4082.

458 [21] J.L. Cohen, D.J. Volpe, D.A. Westly, A. Pechenik, H.D. Abruña, A dual electrolyte H<sub>2</sub>/O<sub>2</sub>  
459 planar membraneless microchannel fuel cell system with open circuit potentials in excess of 1.4  
460 V, *Langmuir*, 21 (2005) 3544-3550.

461 [22] S. Cheng, K.-Y. Chan, High-Voltage Dual Electrolyte Electrochemical Power Sources, *ECS*  
462 *Transactions*, 25 (2010) 213-219.

463 [23] H. Li, C. Oloman, Development of a continuous reactor for the electro-reduction of carbon  
464 dioxide to formate—Part 1: Process variables, *Journal of Applied Electrochemistry*, 36 (2006)  
465 1105-1115.

466 [24] H. Li, C. Oloman, The Electro-Reduction of Carbon Dioxide in a Continuous Reactor,  
467 *Journal of Applied Electrochemistry*, 35 (2005) 955-965.

468 [25] F. Köleli, T. Atilan, N. Palamut, A.M. Gizir, R. Aydin, C.H. Hamann, Electrochemical  
469 reduction of CO<sub>2</sub> at Pb- and Sn-electrodes in a fixed-bed reactor in aqueous K<sub>2</sub>CO<sub>3</sub> and  
470 KHCO<sub>3</sub> media, *Journal of Applied Electrochemistry*, 33 (2003) 447-450.

471 [26] H. Zhang, M.K.H. Leung, J. Xuan, H. Xu, L. Zhang, D.Y.C. Leung, H. Wang, Energy and  
472 exergy analysis of microfluidic fuel cell, *International Journal of Hydrogen Energy*, 38 (2013)  
473 6526-6536.

474 [27] H. Wang, D.Y.C. Leung, J. Xuan, Modeling of a micro auto-electrolytic cell for hydrogen  
475 production, *International Journal of Hydrogen Energy*, 37 (2012) 10009.

476 [28] K. Hsieh, A.S. Patterson, B.S. Ferguson, K.W. Plaxco, H.T. Soh, Rapid, Sensitive, and  
477 Quantitative Detection of Pathogenic DNA at the Point of Care through Microfluidic  
478 Electrochemical Quantitative Loop-Mediated Isothermal Amplification, *Angewandte Chemie*,  
479 124 (2012) 4980-4984.

480 [29] Y. Wu, P. Xue, K.M. Hui, Y. Kang, A paper-based microfluidic electrochemical  
481 immunodevice integrated with amplification-by-polymerization for the ultrasensitive  
482 multiplexed detection of cancer biomarkers, *Biosensors and Bioelectronics*, 52 (2014) 180-187.

483 [30] G.P. Roth, R. Stalder, T.R. Long, D.R. Sauer, S.W. Djuric, Continuous-flow microfluidic  
484 electrochemical synthesis: investigating a new tool for oxidative chemistry, *Journal of Flow  
485 Chemistry*, 3 (2013) 34-40.

486 [31] S. Sabatino, A. Galia, O. Scialdone, Electrochemical Abatement of Organic Pollutants in  
487 Continuous-Reaction Systems through the Assembly of Microfluidic Cells in Series,  
488 *ChemElectroChem*, 3 (2016) 83-90.

489 [32] D. Voicu, M. Abolhasani, R. Choueiri, G. Lestari, C. Seiler, G. Menard, J. Greener, A.  
490 Guenther, D.W. Stephan, E. Kumacheva, Microfluidic studies of CO<sub>2</sub> sequestration by frustrated  
491 Lewis pairs, *Journal of the American Chemical Society*, 136 (2014) 3875-3880.

492 [33] H. Wang, D.Y.C. Leung, J. Xuan, Modeling of a microfluidic electrochemical cell for CO<sub>2</sub>  
493 utilization and fuel production, *Applied Energy*, 102 (2013) 1057-1062.

494 [34] M. Abolhasani, A. Günther, E. Kumacheva, Microfluidic studies of carbon dioxide,  
495 *Angewandte Chemie International Edition*, 53 (2014) 7992-8002.

496 [35] K. Wu, E. Birgersson, B. Kim, P.J. Kenis, I.A. Karimi, Erratum: Modeling and  
497 Experimental Validation of Electrochemical Reduction of CO<sub>2</sub> to CO in a Microfluidic Cell [*J.  
498 Electrochem. Soc.*, 162, F23 (2015)], *Journal of The Electrochemical Society*, 162 (2015) X6-X6.

499 [36] D.T. Whipple, E.C. Finke, P.J.A. Kenis, Microfluidic reactor for the electrochemical  
500 reduction of carbon dioxide: The effect of pH, *Electrochemical and Solid-State Letters*, 13 (2010)  
501 B109-B111.

502 [37] E.R. Choban, J.S. Spendelow, L. Gancs, A. Wieckowski, P.J.A. Kenis, Membraneless  
503 laminar flow-based micro fuel cells operating in alkaline, acidic, and acidic/alkaline media,  
504 *Electrochimica Acta*, 50 (2005) 5390-5398.

505 [38] A. Boddien, D. Mellmann, F. Gärtner, R. Jackstell, H. Junge, P.J. Dyson, G. Laurenczy, R.  
506 Ludwig, M. Beller, Efficient dehydrogenation of formic acid using an iron catalyst, *Science*, 333  
507 (2011) 1733-1736.

508 [39] C. Rice, S. Ha, R.I. Masel, P. Waszczuk, A. Wieckowski, T. Barnard, Direct formic acid  
509 fuel cells, *Journal of Power Sources*, 111 (2002) 83-89.

510 [40] X. Yu, P.G. Pickup, Recent advances in direct formic acid fuel cells (DFAFC), *Journal of  
511 Power Sources*, 182 (2008) 124-132.

512 [41] N. Sridhar, D. Hill, Carbon dioxide utilization Electrochemical conversion of CO<sub>2</sub> –  
513 Opportunities and Challenges, in: Research and Innovation, Position Paper, Det Norske vertas,  
514 Høvik, Norway, 2011.

515 [42] A.S. Agarwal, Y. Zhai, D. Hill, N. Sridhar, The electrochemical reduction of carbon dioxide  
516 to formate/formic acid: Engineering and economic feasibility, *ChemSusChem*, 4 (2011) 1301-  
517 1310.

518 [43] T. Reda, C.M. Plugge, N.J. Abram, J. Hirst, Reversible interconversion of carbon dioxide  
519 and formate by an electroactive enzyme, *Proceedings of the National Academy of Sciences*, 105  
520 (2008) 10654-10658.

521 [44] S.K. Lower, Acid-base equilibria and calculations, in, *A Chem*, 2014.

522 [45] Y. Hori, S. Suzuki, Electrolytic reduction of carbon dioxide at mercury electrode in aqueous  
523 solution, *Bulletin of the Chemical Society of Japan*, 55 (1982) 660-665.

524 [46] C. Sanchez-Sanchez, V. Montiel, D. Tryk, A. Aldaz, A. Fujishima, Electrochemical  
525 approaches to alleviation of the problem of carbon dioxide accumulation, *Pure and Applied*  
526 *Chemistry*, 73 (2001) 1917-1927.

527 [47] N. Gupta, M. Gattrell, B. MacDougall, Calculation for the cathode surface concentrations in  
528 the electrochemical reduction of CO<sub>2</sub> in KHCO<sub>3</sub> solutions, *Journal of Applied Electrochemistry*,  
529 36 (2006) 161-172.

530 [48] R. Sleat, R.A. Mah, Quantitative method for colorimetric determination of formate in  
531 fermentation media, *Applied and environmental microbiology*, 47 (1984) 884.

532 [49] H. Li, C. Oloman, Development of a continuous reactor for the electro-reduction of carbon  
533 dioxide to formate – Part 2: Scale-up, *Journal of Applied Electrochemistry*, 37 (2007) 1107-1117.

534 [50] X. Lu, D.Y. Leung, H. Wang, M.K. Leung, J. Xuan, Electrochemical reduction of carbon  
535 dioxide to formic acid, *ChemElectroChem*, 1 (2014) 836-849.

536 [51] T. Reier, M. Oezaslan, P. Strasser, Electrocatalytic oxygen evolution reaction (OER) on Ru,  
537 Ir, and Pt catalysts: a comparative study of nanoparticles and bulk materials, *Acs Catalysis*, 2  
538 (2012) 1765-1772.

539 [52] X. Min, M.W. Kanan, Pd-catalyzed electrohydrogenation of carbon dioxide to formate:  
540 High mass activity at low overpotential and identification of the deactivation pathway, *Journal of*  
541 *the American Chemical Society*, 137 (2015) 4701-4708.

542 [53] A. Del Castillo, M. Alvarez-Guerra, J. Solla-Gullón, A. Sáez, V. Montiel, A. Irabien,  
543 Electrocatalytic reduction of CO<sub>2</sub> to formate using particulate Sn electrodes: Effect of metal  
544 loading and particle size, *Applied Energy*, 157 (2015) 165-173.

545 [54] T.M.a.S.I. K. Ito, Electrochemical reduction of carbon dioxide on zinc and cadmium  
546 electrodes, *Zh. Prikl. Khim.*, *Bulletin of the Nagoya Institute of Technology*, 209-214 (1975).

547 [55] F. Köleli, D. Balun, Reduction of CO<sub>2</sub> under high pressure and high temperature on Pb-  
548 granule electrodes in a fixed-bed reactor in aqueous medium, *Applied Catalysis A: General*, 274  
549 (2004) 237-242.

550 [56] Y. Chen, M.W. Kanan, Tin oxide dependence of the CO<sub>2</sub> reduction efficiency on tin  
551 electrodes and enhanced activity for tin/tin oxide thin-film catalysts, *Journal of the American*  
552 *Chemical Society*, 134 (2012) 1986-1989.

553 [57] J. Wu, F.G. Risalvato, F.-S. Ke, P. Pellechia, X.-D. Zhou, Electrochemical reduction of  
554 carbon dioxide I. Effects of the electrolyte on the selectivity and activity with Sn electrode,  
555 *Journal of The Electrochemical Society*, 159 (2012) F353-F359.



556 [58] S. Grigoriev, P. Millet, V. Fateev, Evaluation of carbon-supported Pt and Pd nanoparticles  
557 for the hydrogen evolution reaction in PEM water electrolyzers, *Journal of Power Sources*, 177  
558 (2008) 281-285.

559 [59] M. Carmo, D.L. Fritz, J. Mergel, D. Stolten, A comprehensive review on PEM water  
560 electrolysis, *International Journal of Hydrogen Energy*, 38 (2013) 4901-4934.

561 [60] Y. Hori, H. Wakebe, T. Tsukamoto, O. Koga, Electrocatalytic process of CO selectivity in  
562 electrochemical reduction of CO<sub>2</sub> at metal electrodes in aqueous media, *Electrochimica Acta*,  
563 39 (1994) 1833-1839.

564 [61] R. Williams, R.S. Crandall, A. Bloom, Use of carbon dioxide in energy storage, *Applied*  
565 *Physics Letters*, 33 (1978) 381-383.

566 [62] C. Oloman, H. Li, Electrochemical processing of carbon dioxide, *Chemosuschem*, 1 (2008)  
567 385-391.

568 [63] Lu X, Xuan J, Leung DYC, Zou HY, Li JT, Wang HL, a.W. HZ, A switchable pH-  
569 differential unitized regenerative fuel cell with high power density and round-trip efficiency,  
570 *Journal of Power Sources*, 314 (2016) 76-84.

571 [64] S. Druckmann, M. Ottolenghi, A. Pande, J. Pande, R. Callender, Acid-base equilibrium of  
572 the Schiff base in bacteriorhodopsin, *Biochemistry*, 21 (1982) 4953-4959.

573 [65] J. Kobayashi, Y. Mori, K. Okamoto, R. Akiyama, M. Ueno, T. Kitamori, S. Kobayashi, A  
574 microfluidic device for conducting gas-liquid-solid hydrogenation reactions, *Science*, 304 (2004)  
575 1305-1308.

576 [66] D.T. Whipple, P.J.A. Kenis, Prospects of CO<sub>2</sub> Utilization via Direct Heterogeneous  
577 Electrochemical Reduction, *The Journal of Physical Chemistry Letters*, 1 (2010) 3451-3458.

578 [67] X. Huang, C.J. Margulis, Y. Li, B.J. Berne, Why is the partial molar volume of CO<sub>2</sub> so  
579 small when dissolved in a room temperature ionic liquid? Structure and dynamics of CO<sub>2</sub>  
580 dissolved in [Bmim<sup>+</sup>][PF<sub>6</sub><sup>-</sup>], *Journal of the American Chemical Society*, 127 (2005) 17842-  
581 17851.

582 [68] Á. Pérez-Salado Kamps, D. Tuma, J. Xia, G. Maurer, Solubility of CO<sub>2</sub> in the ionic liquid  
583 [bmim][PF<sub>6</sub>], *Journal of Chemical & Engineering Data*, 48 (2003) 746-749.

584 [69] J. Kumelan, Á.P.-S. Kamps, D. Tuma, G. Maurer, Solubility of CO<sub>2</sub> in the ionic liquids  
585 [bmim][CH<sub>3</sub>SO<sub>4</sub>] and [bmim][PF<sub>6</sub>], *Journal of Chemical & Engineering Data*, 51 (2006) 1802-  
586 1807.

587

588